Quokka Swarm Driven PI Controller for High-Performance PV Microgrid with Interleaved Boost Converter

N. Janaki
Department of Electrical and Electronics Engineering
Vels Institute of Science, Technology and Advanced Studies,
Chennai, India.
jn4004528@gmail.com

Arunagiri A
Department of Electrical and Electronics Engineering
Vels Institute of Science, Technology and Advanced Studies,
Chennai, India.
freakiisparkler@gmail.com

Mohudhoom Basith M
Department of Electrical and Electronics Engineering
Vels Institute of Science, Technology and Advanced Studies,
Chennai, India.
joysman35@gmail.com

Vignesh G
Department of Electrical and Electronics Engineering
Vels Institute of Science, Technology and Advanced Studies,
Chennai, India.
viki.vistas@gmail.com

***Abstract*— Over last decade, energy utilization based on Renewable Energy Source (RES) has grown significantly by more than 10% each year. In addition to that, aiming at better overall grid efficiency and reliability, this study presents a new decentralized output-constrained control algorithm for Direct Current (DC) Micro Grids (MGs). It involves the study of PV integration in MG. The low voltage coming from the solar source is elevated by DC-DC converters. This paper presents an Interleaved Boost Converter (IBC) for raising the energy from the PV modules when they are in need of high voltage for an efficient DC microgrid operation. The suggested converter attaches PV modules as separate sources, provides high-efficiency and a significant voltage conversion ratio with the minimal use of the components. In order to improve power quality and achieve higher system efficiency, the control strategy needs to be of great importance. QSO-optimized PI controllers are utilized to provide stable and dynamic power even during irradiance fluctuations. The proposed model for upgrading PV microgrid systems is implemented in MATLAB/Simulink and simulation results confirm that IBC converter reach an efficiency of 94.17% with a higher gain than the traditional converters, simplified control mechanisms, and reduced energy losses with THD of 0.62%.**

Keyword—Microgrid, PV system, IBC, Quokka Swarm optimized PI controller, MATLAB.

I. INTRODUCTION

Increasing costs of fossil fuels and the need to decarbonize the energy sector have revitalized the discussion about scaling up energy production from RES. However, intermittent nature of RES leads to problems in continuous and stable usage, thus there are mismatches between when the power is available and is consumed by the end-users. The effectiveness and stability of these systems can be greatly improved by coupling energy storage with RES-based power generators [1]. Decentralized and distributed power generation systems, such as microgrids, are growing in popularity as viable solutions to the problem of limited RES-based power production. Microgrids facilitate the development of smaller and more flexible power networks that can either function autonomously or be interconnected with larger central grids for the power exchange as needed [2]. These systems provide increased efficiency, resource optimization, and almost zero carbon emissions. In addition, microgrids integrate numerous loads, such as different types of buildings (residential, commercial, public, and industrial). In comparison with conventional auxiliary power units (APUs) that are typically employed in remote applications, microgrids have the capability to give better operational flexibility and lower carbon emissions [3]. Direct Current (DC) microgrids are becoming more and more popular as a result of their adaptability in various fields, such as EVs. Researchers are prioritizing investigation of DC MG systems due to increasing need for sustainable energy [4].

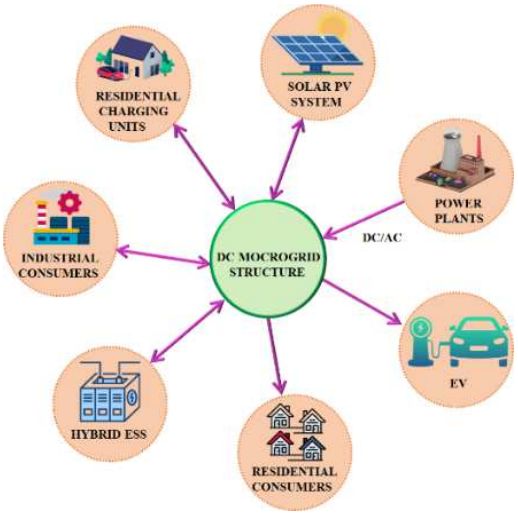

Fig. 1. Overall system layout for the proposed microgrid.

Figure 1 depicts layout of DC microgrid, showcasing its connections to power generation systems, RES energy storage systems, and diverse loads like EV and smart buildings. These systems integrate diverse RES including solar, wind, and fuel cells, coupled with DC converter to optimize performance and stabilize voltage fluctuations [5-6]. Boost Converter increase the output voltage to achieve specific value of DC voltage. However, it is heavily relies on dynamic solar irradiation conditions [7]. Cascaded Boost Converter increase the voltage gain, it further enhances the reliability and stability in the integration RES based systems. Nevertheless, it introduces additional switching losses which hinders the overall efficiency of the system [8]. Quadratic Boost Converter offer extensive voltage gain using a minimal number of components. Nonetheless, the high voltage gain result in elevated voltage stress on switching devices limiting

practical applicability [9]. This paper proposes a novel IBC that effectively boost DC power from solar systems. Control algorithms are required to regulate operations of converter. PI controller is equipped that produces the error signal by comparing actual and reference power values from PV system for IBC controlling operations. Leveraging optimization further enhance the control algorithm.

TABLE I. OPTIMIZATION ALGORITHMS LITERATURE REVIEW:

Ref	Control Method	Optimization Methodology	Contributions
[10]	ABC	Artificial Bee Colony	A bio-inspired approach that leverages collective foraging behavior of honeybees to regulate output voltage of PV module under fluctuating irradiance and ambient temperature conditions.
[11]	GHO	Grasshopper Optimization.	GH optimization improves the stability of systems when faced with fluctuating conditions.
[12]	SSA	Salp Swarm Based MPPT	Bioinspired optimization algorithms, based on the swarming behavior of salp groups during ocean foraging and navigation.

However, these optimization algorithms have limitations such as parameter sensitivity, and risks of premature convergence. These drawbacks are overcome by proposed QSO algorithm. It finds the optimal solution within a defined search space. Specifically, the QSO algorithm identifies the best PI parameters to minimize the error between V_{ref} and V_{DC}. Thus, the proposed model improves overall system reliability and robustness, better ability to manage non-linearity within the system, and adaptability to varying input conditions make QSO controller an ideal choice for integrating RES into resilient MGs.

A. Research gap

The analysis reveals a significant gap in the research area regarding the integration of resilient hybrid controllers and innovative meta-heuristic optimization algorithms, particularly in uncertain scenarios. The comprehensive examination of current studies and experimental results points to this gap, which is central to the emphasis of the control methods of the future. Such methods ought to utilize the synergistic benefits of controllers and meta-heuristic optimization algorithms improving reliability which are subjected to random operating conditions. It is a crucial step forward in the discipline to connect this gap, thus establishing the basis for subsequent research and application.

B. Research motivation

The limitations of control strategies for MGs highlight an urgent requirement for advances in this area. The current study intends to go halfway between new theoretical concepts and their real application in the design of optimized controllers for MGs. Encouraged by a comprehensive approach, the work intends to move forward this important area by solving the research gaps that have been identified. The new QS optimization framework proposed is intended to be strong and adaptable, thus it can provide better system performance and a reliable power supply for isolated communities. Besides offering feasible solutions, this study also intends to become a part of the academic debate on the development of control strategies for MGs and to make a positive contribution in the form of insights.

C. Major contributions

- IBC converter boosts the voltage of solar panels, decreases current and voltage ripple, and improves efficiency, resulting in consistent power output appropriate for grid connection.
- PI controller handles active and reactive power flow in outer control loop, ensuring that MG operates at the required power factor while meeting grid requirements.
- QSO algorithm improves the PI controller system reliability by effective hyperparameters tuning.

Following the introduction, Section II details block diagram of MG system. Section III presents modelling of proposed system, while Section IV outlines experimental results. A comparative analysis of IBC efficiency and THD against conventional converters is provided in Section V. Finally, Section VI concludes study with key findings and implications

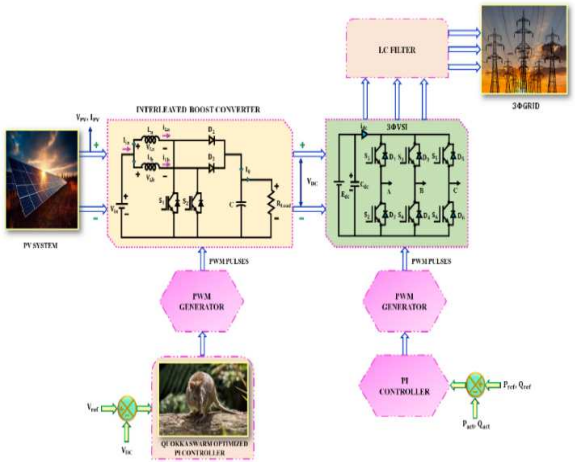

Fig. 2. Schematic representation of the proposed system architecture.

A MG incorporates PV modules, IBC, QS optimized PI controller, PWM generator and 3Φ VSI . Fig. 2 illustrates the primary components involved in designing the proposed MG model. The PV system produces DC power by extracting solar energy from the sun. Output power of PV panels is fed GBC, which produces high power with reduced ripple and improved efficiency. The converter operations are controlled by the optimized PI controller. It takes actual V_{ref} and V_{DC}, compare with reference value, generates error signal. The performance of the PI controller is further enhanced by the QS optimization algorithm which optimally tunes the model hyperparameters. In proposed system, QS-optimized PI controller generates control signals that are fed into The enhanced DC power is then supplied to 3Φ VSI, transforms it into AC power suitable for MG applications. The operation of the VSI is also governed by the PWM generator, which receives reference signals from the PI controller to maintain synchronized and stable AC output. This integrated control strategy enables seamless and reliable PV system incorporation into the MG framework. A detailed explanation of each subsystem and its functional role is provided in the following subsections.

II. Proposed System Modelling.

Solar PV modules harness sunlight and convert it directly into electrical energy. To meet specific power requirements, these modules are typically configured by interconnecting solar cells in both series and parallel arrangements. Among available PV technologies, monocrystalline and polycrystalline variants are most widely adopted due to their efficiency and reliability in diverse environmental conditions. Figure 3 presents a schematic representation of this PV model.

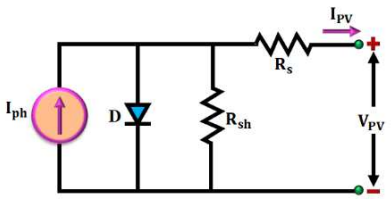

Fig. 3. PV cell equivalent circuit.

Voltage–current (V–I) behavior of a PV cell is governed by a nonlinear equation, mathematically represented as:

$$I_{PV} = I_{PH} - I_S e^{\left(\frac{q(V_{PV}+R_S I_{PV})}{nKT}-1\right)} - \frac{V_{PV}+R_S I_{PV}}{R_{SH}} \quad (1)$$

Here, I_{PH} denotes photo-generated current, while I_S refers to diode's saturation current. Term q represents elementary charge of an electron, T is absolute temperature in Kelvin, and n is ideality factor of P–N junction. Parameters R_S and R_{SH} parallel resistance, respectively. To enhance output power derived from PV system, a DC–DC converter is employed, which efficiently boosts voltage and regulates power flow under varying environmental conditions.

A. Interleaved Boost Converter

IBC produces high voltage from getting power by PV system, comprising of S_1 andS_2 switches, inductors L_a andL_b , diodes D_1 andD_2, a capacitor$C$, and a load resistorR_o, powered by a reliable input source V_S. Equivalent circuit of IBC is given in Fig. 4. Switches are controlled using phase-shifted switching, and the converter operates across four distinct modes. The two inductance values are assumed to be equal (L_a=L_b =L), along with identical duty cycles (D_1= D_2=D) and a corresponding time delay of$(T/2)$.

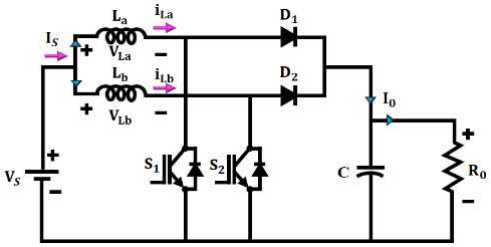

Fig. 4. DC-DC Interleaved Boost Converter.

Mode 1: Here, S_1 and S_2 are closed, schematic of the IBC in this mode is shown in Fig. 5. In this configuration, D_1 and D_2 reverse-biased. During this phase, source powers the inductor L_a and L_b , leading to an increase in inductor currents i_{La} and i_{Lb}.

$$V_{La} = V_S \quad (2)$$

$$V_{Lb} = V_S \quad (3)$$

Where, $V_{La} = L_a \frac{di_{La}}{dt}$ and $V_{Lb} = L_b \frac{di_{Lb}}{dt}$

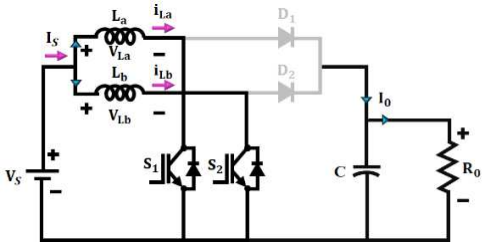

Fig. 5. IBC mode 1 operation.

Mode 2: Switch S_1 is activated (closed) while switch S_2 remains deactivated (open), leading to diode D_1 becoming reverse-biased, whereas D_2 is forward-biased and conducts current. Corresponding schematic of IBC for this mode is depicted in Fig. 6. During this interval, input source energizes inductor L_a, resulting in an increase in its currenti_{La}. This coordinated switching sequence ensures continuous power delivery and efficient energy conversion within the IBC topology.

$$V_{La} = V_S \quad (4)$$

$$V_{Lb} = V_S - V_{out} \quad (5)$$

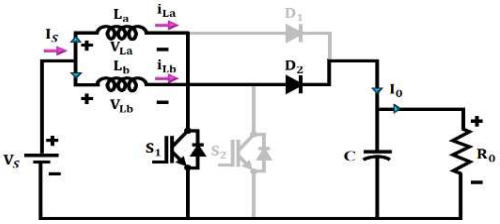

Fig. 6. IBC mode 2 operation.

Mode 3: Switch S_1 is turned OFF while switch S_2 remains ON, resulting in diode D_1 becoming forward-biased and conducting, whereas D_2 is reverse-biased and non-conducting. Corresponding IBC configuration is illustrated in Fig. 7. Under these conditions, inductor L_a releases its stored energy to load, causing a reduction in its current i_{La}. Concurrently, input source energizes inductor L_b, leading to an increase in its current i_{Lb}. This coordinated switching action ensures continuous energy transfer and efficient voltage boosting within IBC topology.

$$V_{La} = V_S - V_{out} \quad (6)$$

$$V_{Lb} = V_S \quad (7)$$

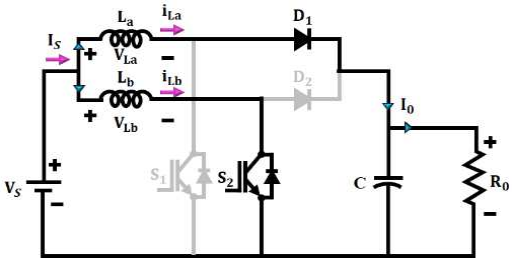

Fig. 7. IBC mode 3 operation.

Mode 4: During this operational mode, S_1 and S_2 remain in OFF state, while D_1 and D_2 conducts. Corresponding circuit configuration is illustrated in Fig. 8. Under these conditions, L_a and L_b discharge, transferring stored energy directly to load. This discharge process leads to a gradual

reduction in inductor currents i_{La} and i_{Lb}. Dynamic behaviour of this current decay is mathematically described by following rate of change expression:

$$V_L = V_S - V_{out} \tag{8}$$

$$\frac{di_{La}}{dt} = \frac{di_{Lb}}{dt} = \frac{V_S - V_{out}}{L} \tag{9}$$

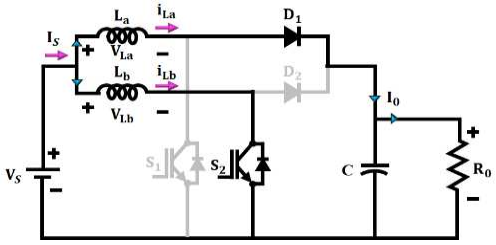

Fig. 8. IBC mode 4 operation.

In steady state operation,

$$V_{out} = \frac{V_S}{(1-\delta)} \tag{10}$$

Minimum inductor value of L_a is L_{a_min}, and L_b is L_{b_min}.

$$L_{a\_min} = L_{b\_min} = \frac{V_{in}\delta T}{2\Delta i_L} \tag{11}$$

The capacitor value C is given by,

$$C_{min} = \frac{\delta}{R\left(\frac{\Delta V_{out}}{V_{out}}\right)f_s} \tag{12}$$

IBC modes of operation waveform is given in Fig. 9

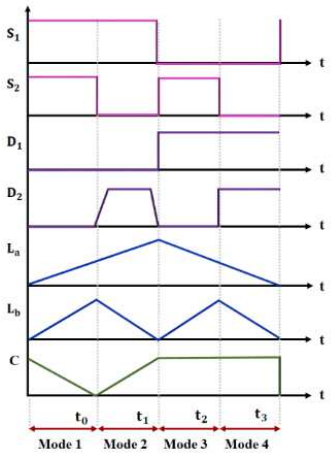

Fig. 9. Switching mode operation of IBC.

The IBC operations are controlled for enhanced power generation. The PI controller generates essential control signal for the IBC.

B. PI Controller

A PI controller is an effective control approach, which is integrated in various applications and is defined by two distinct components: the Proportional (P) and the Integral(I). The proportional parameter governs response to present error, while integral parameter focuses on response derived from accumulation of previous errors. Proportional and integral are represented by K_p and K_t respectively. The output of the controller is $y(t)$. e denotes the voltage error value given to PI controller. PI controller transfer function is given in Fig. 10.

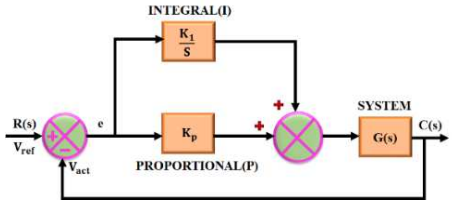

Fig. 10. PI controller

Reference DC link voltage value is proportional to the difference between actual and reference voltage values. Its parameters K_p and K_t are finely tuned with optimization algorithm for further enhancement.

C. Quokka Optimization Algorithm

Quokka is a member of macropod family, that rest during daytime and at night it exhibits increased activity, often gathering near waterholes in groups. Their diet consists of local grasses, leaves, seeds, and roots, which they consume quickly and later regurgitate to chew again, akin to ruminants. During extended dry periods in hot climates, quokkas furthest from water sources face the highest risk of mortality. In addition, it deplete water from plants and produce nitrogen deficiency problems. Insights into their behavior serve as valuable inspiration for the proposed optimized PI controller technique.

1) Social interaction.
2) Adaptability.
3) Exploration and foraging.

D. Mathematical modelling

Each position of quokkas within group gets influenced by position of best quokka within than group, expressed by following equation

$$D_{new} = \frac{(T+H)}{(0.8\times D^{old})} + \Delta w \times rand \times \Delta X, \tag{13}$$

$$X^{new} = X^{old} + D^{new} \times N, \tag{14}$$

Drought is represented by D^{old} the value ranges between $[0, 1]$, ratio of temperature is $T(0.2 - 0.44)$ and H is humidity ratio. These ranges are selected as they align with the condition's quokkas tolerate. Parameter Δw represents difference in weight between leader and quokka i, ΔX indicates the positional gap between them. Term $rand$ refers to a randomly generated value within the range $[0, 1]$. Updated position of a quokka is denoted as X^{new} and its previous position is X^{old} to its previous position. N stands for nitrogen ratio a crucial factor influencing quokka behavior, which varies between 0 and 1. Lower nitrogen values negatively impact quokkas, increasing dehydration risks, whereas higher values are more beneficial. Constant 0.8 in first equation ensures that combined temperature and humidity levels remain within tolerable limits, as quokkas not withstand extreme heat and humidity. The QSO algorithm simulates quokka behavior and outlines its pseudo-code. Initially, in exploratory mode, random solutions are generated, and their fitness is evaluated. Values for temperature, humidity, and nitrogen are then initialized. As algorithm reaches enhanced solutions, it transits to local exploitation phase, focusing on promising regions within the search space. During this phase, quokka exhibits highest fitness value by the leader. Following this, search agents reinitiate exploratory movements, marking the onset of new exploitation cycle. Humidity and position of each quokka are

then updated based on equations (13) and (14) with leaders fitness guiding the recalibration of all agents fitness value.

Once the stopping condition is met, the process concludes, presenting leader as best approximation for solving optimization problem. Figure 11 illustrates QSO algorithm's flowchart.

Thus, QSO algorithm effectively tunes the controller parameters. Thus, the proposed model enhances the performance of high-efficiency PV microgrids by optimizing the control parameters of the IBC. This integration ensures stable DC link voltage, improved power quality, and system reliability, making it ideal for high-performance applications.

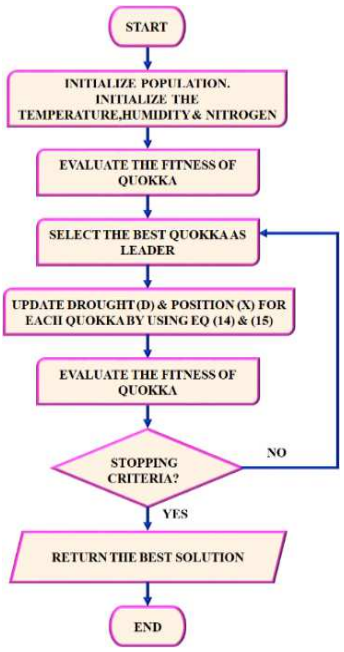

Fig. 11. Flowchart of QSO.

III. Result And Discussion

The outcomes of presented approach, which is implemented in MATLAB/Simulink, are discussed below. The PV and IB converter parameter specifications are shown in Table II.

TABLE II. Simulation Setup Parameters And Values

Parameter	Specification
PV system	
Rated Power	$10kW$
No. of panels arranged in series	6
No. of panels arranged in parallel	7
Short circuit current	$8.3A$
Open circuit voltage	$12V$
IBC	
Inductor L_a, L_b	$4.7mH$
Capacitor C	$22\mu F$
Switching Frequency	$10kHz$

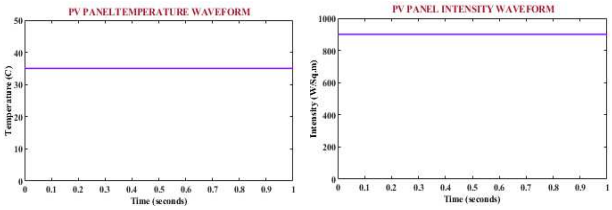

Fig. 12. PV panel waveform.

Figure 12 presents the PV panel waveform over a duration of $1\ s$. Figure 12. (a) shows temperature waveform of PV system. Temperature steadily maintained 35^0C. Figure 12 (b) shows intensity waveform of PV panel. The intensity is stabilized at a constant level of $900(W/sq.m)$. These consistent readings exhibit stable operating conditions for a PV microgrid system, where both temperature and intensity are effectively controlled.

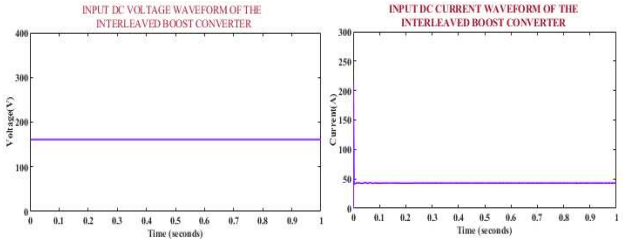

Fig. 13. Input waveforms of IBC.

Figure 13 represents the IBC input waveforms. Figure 13 (a) shows the input DC voltage waveform of IBC, indicating consistent DC input voltage of $170V$.Converter's input DC current waveform is displayed in Fig. 13 (b). A steady DC input current of 45A is reached after current first exhibits minor oscillations.

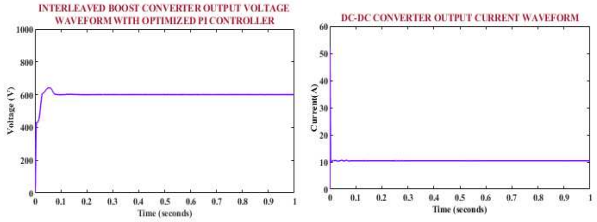

Fig. 14. Output waveform of IBC.

Figure 14 displays the IBC output waveforms. Converter output DC voltage waveform is displayed in Fig. 14 (a).In initial phase, voltage overshoot and stabilize around $600V$. Figure 14 (b) shows the DC converter output current waveform. Constant current of $12A$ is maintained.

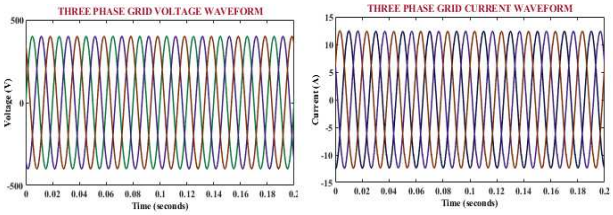

Fig. 15. 3Φ grid waveforms.

3Φ grid voltage and current waveform is shown in Fig. 15. Voltage waveform of 3Φ grid is displayed in Fig. 15 (a). A well-balanced sinusoidal voltage waveform is attained where the voltage ranges from $-500V$ to $+500V$. Figure 15 (b) shows the current waveform of 3Φ grid. It represents a steady current flow of $15A$.

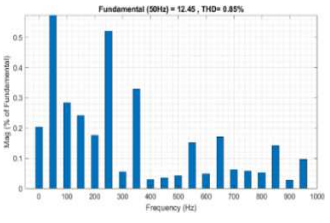

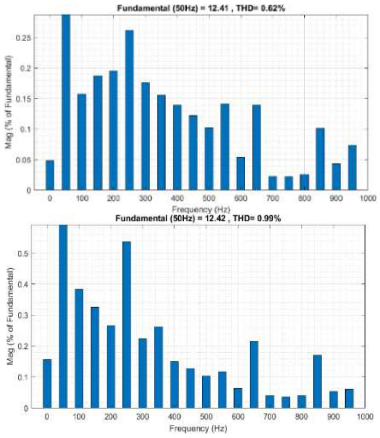

Fig. 16. THD Waveform for 3 phases.

Figure 16 demonstrates the THD waveform for the three phases. The fundamental frequency 50 Hz has a magnitude of 12.45, 12.41 and 12.42, and the THD is 0.85%, 0.62% and 0.99% for R, Y and B phases respectively. The lower value of THD exhibits enhanced quality of power delivered to the grid.

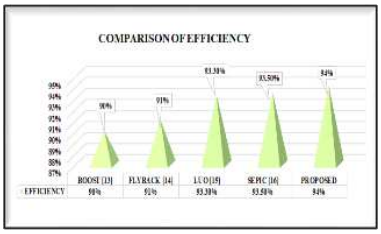

Fig. 17. Comparison of efficiency.

Figure 17 illustrates the comparison of converter efficiency. Proposed IBC archives enhanced efficiency of 94.17% outperforming conventional converters such as Boost converter at 90%, flyback converter at 91%, Luo converter at 93.3% and SEPIC converter at 93.5%. Thus, highlighting the proposed converter enhancing efficiency in PV microgrid applications.

TABLE III. COMPARISON OF THD.

Converter	THD
Buck-Boost[17]	8.66%
Dual Boost Converter [18]	9.11%
Proposed	0.62%

Table III presents the comparative analysis of THD. From the table, proposed converter achieves a remarkably low THD of 0.62%, outperforming the Buck-Boost converter [17] with 8.66% and the Dual Boost Converter with [18] 9.11%. From the table, proposed approach signifies as highly effective in reducing harmonics in MG system.

IV. CONCLUSION

This research proposes the a novel PV integrated system in improving the performance of MG. The high enhanced DC power is attained by capturing low voltage from PV panels to elevated levels by the IBC. The converter operations are effectively controlled by PI controller and its performance is further optimized QSO algorithm, ensuring that the system performs in effectively in fluctuating conditions. A key benefit of developed converter lies in its capability to manage multiple power sources, thereby enhancing energy efficiency and operational reliability within microgrid environments. Overall, this approach supports a more sustainable and resilient energy infrastructure by improving power system efficiency and promoting wider integration of RES. The enhanced IBC converter attains a peak efficiency of 94.17% and significantly minimized THD of 0.62%.

REFERENCE

[1] S. Karthick, M. Ramesh Babu, M. Shyam, B. Jeyapoornima, S. R and S. Gomathi, "Stability Analysis of Integrated Power System with Renewable Energy Sources," 2023 Second International Conference on Electronics and Renewable Systems (ICEARS), Tuticorin, India, pp. 185-190, 2023.

[2] O. M. Basel, "Integrating Renewable Energy Systems into Urban Planning for Sustainable Cities,"ESTIDAMAA, no. 2024, pp. 15-21, 2024.

[3] A. S. Abdulbaqi and S. M. N. Nejrs, "Innovative control strategies for dynamic load management in smart grid techniques incorporating renewable energy sources," Khwarizmia, no. 2023, pp. 73-83, 2023.

[4] K. S. Kavin and P. Subha Karuvelam, "A novel KSK converter with machine learning MPPT for PV applications," Electric Power Components and Systems, pp. 1-19, 2024.

[5] P. S.Shama, P. C. Sekhar, S. Shinde, G. Kalnoor, and B. Gireesha, "An optimized operation of hybrid Wind/Battery/PV-System based micro grid by using particle swarm optimization technique," Journal of Computational Information Systems, vol. 14, no. 5, pp. 79-84, 2018.

[6] A. K. Wadhwani, "High performance adaptive PSO MPPT technique for PV based micro grid for a rural area," In Journal of Physics: Conference Series, vol. 1817, no. 1, pp. 012026, IOP Publishing, 2021.

[7] H. T. Nguyen, "Boost-converter reliability assessment for renewable-energy generation systems in a low-voltage DC microgrid," energy Reports, no. 8, pp. 821-835, 2022.

[8] V. S. Rao, "Performance analysis of voltage multiplier coupled cascaded boost converter with solar PV integration for DC microgrid application," IEEE Transactions on Industry Applications, vol. 59, no. 1, pp. 1013-1023, 2022.

[9] N. V. Sivaram and A. Lavanya, "Dual input single Output quadratic Boost converter for DC microgrid," e-Prime-Advances in Electrical Engineering, Electronics and Energy, no. 9, pp. 100683, 2024.

[10] R. Sugumar, "A hybrid modified artificial bee colony (ABC)-based artificial neural network model for power management controller and hybrid energy system for energy source integration," 2023.

[11] K. Aseem, "Hybrid k-means Grasshopper Optimization Algorithm based FOPID controller with feed forward DC–DC converter for solar-wind generating system," Journal of Ambient Intelligence and Humanized Computing, pp. 1-24, 2022.

[12] Z. Albataineh, "Optimization of fractional order PI controller to regulate grid voltage connected photovoltaic system based on slap swarm algorithm," Int. J. Power Electron. Drive Syst. (IJPEDS), vol. 14, no. 2, pp. 1184, 2023.

[13] N. Subhani, "An improved non-isolated quadratic DC-DC boost converter with ultra-high gain ability," IEEE Access, no. 11, pp. 11350-11363, 2023.

[14] S. J. Yaqoob, "Flyback photovoltaic micro-inverter with a low cost and simple digital-analog control scheme," Energies, vol. 14, no. 14, pp. 4239, 2021.

[15] R. Banupriya, "Performance Analysis of a Relift Luo Converter-Derived Dual-Output DC to DC Converter for Microgrid Applications," International Journal of Photoenergy, vol. 2022, no. 1, pp. 8093589, 2022.

[16] M. Tanashu, "Design and Analysis of Low-Cost and Efficient SEPIC Converter for Affordable Solar Water Pump in Ethiopia," International Journal of Engineering Research in Africa, no. 72, pp. 47-69, 2024.

[17] K. Javed, "Efficiency and Transfer function calculation of the Buck-Boost converter with ideal flow control," In 2021 23rd European Conference on Power Electronics and Applications (EPE'21 ECCE Europe), pp. 1-10, 2021.

[18] P. V. Prasuna, "Improvement in power factor & THD Using dual boost converter," International Journal of Engineering Research and Applications (IJERA), vol. 2, no. 4, pp. 2368-2376, 2012.